Pseudostate methods and differential cross sections for antiproton ionization of atomic hydrogen and helium

M. McGovern,[1] D. Assafrão,[2] J. R. Mohallem,[2] Colm T. Whelan,[3] and H. R. J. Walters[1]

[1]*Department of Applied Mathematics and Theoretical Physics, Queen's University, Belfast BT7 1NN, United Kingdom*

[2]*Laboratório de Átomos e Moléculas Especiais, Departamento de Física, ICEx, Universidade Federal de Minas Gerais, P. O. Box 702, 30123-970 Belo Horizonte, MG, Brazil*

[3]*Department of Physics, Old Dominion University, Norfolk, Virginia 23529-0116, USA*

(Received 20 November 2009; published 29 March 2010)

A relaxed form of a recent impact parameter coupled pseudostate approximation of McGovern *et al.* [Phys. Rev. A **79**, 042707 (2009)] for calculating differential ionization cross sections is proposed. This greatly eases the computational burden in cases where a range of ejected electron energies has to be considered. The relaxed approximation is tested against exact first Born calculations for antiproton impact on H and nonperturbatively for the highly nonperturbative system of Au^{53+} incident upon He. The approximation performs well in these tests. It is shown how, with a little further approximation, the relaxed theory leads to a widely used prescription for the total ionization cross section. Results for differential ionization of H and He by antiprotons are presented. These reveal the growing dominance of the interaction between the antiproton and the target nucleus at low impact energies and show the changing importance of the role of the postcollisional interaction between the antiproton and the ejected electron.

DOI: 10.1103/PhysRevA.81.032708 PACS number(s): 34.10.+x, 34.50.Fa

I. INTRODUCTION

At the European Centre for Nuclear Research (CERN) a large amount of effort is being devoted to the study of antiproton collisions with atomic and molecular targets [1–3]. In addition, the Facility for Antiproton and Ion Research (FAIR) [4] will soon be coming online and so antiproton collisions are also of considerable interest to the FLAIR [5] and SPARC [6] international collaborations.

There are a number of substantive reasons for studying antiproton collisions: as a fundamental process in its own right which presents to theory a stringent test which is "clean" in that it does not involve the complication of identical fermions or electron exchange between the projectile and the target; as an important complement to the study of antihydrogen, which is relevant to proposed fundamental antimatter tests of the CPT invariance of relativistic quantum mechanics and the weak equivalence principle of general relativity [7–10]; as an aid to understanding antiproton reactions in the biological context of antiproton radiotherapy [11].

So far, only measurements of total ionization cross sections have been made, but there are plans for kinematically complete differential ionization experiments [1,12]. Yet, even for total cross-section measurements theoretical information on differential scattering at as detailed a level as possible is valuable in planning the experiments [13].

In a recent publication [14] we developed a highly accurate method for calculating differential ionization by antiprotons. The technique was based on impact parameter pseudostate close-coupling. A downside to the formulation was that a new set of pseudostates had to be generated, and the associated coupled equations re-solved, for each ejected electron energy. The technique becomes tedious in cases where a whole range of ejected energies is needed, which is the case in many experimental situations, e.g., [15–17]. The question is, can we, without significant loss of accuracy, relax the theory so that a single set of pseudostates, and a single solution of the corresponding coupled equations, can be used for all ejected energies of consequence. We shall show that this seems to be the case and that the new formulation leads to convenient formulas for differential cross sections of interest. We shall also show how it justifies a widely used prescription for the total ionization cross section and what further approximations are needed to make this connection.

Having established the viability of the relaxed approximation, we proceed to calculate some cross sections of experimental interest [13] for targets of H and He. Here we are able to generate a more comprehensive picture of the collision process than in Ref. [14], a picture that highlights the important physical behavior.

We begin in Sec. II by describing the relaxation of the approximation of Ref. [14]. In Sec. III we make a number of tests of the relaxed theory and in Sec. IV we present some results on antiproton ionization of H and He. Conclusions are summarized in Sec. V. Throughout we use atomic units (a.u.) in which $\hbar = m_e = e = 1$.

II. THEORY

A. The relaxed approximation

We start from the fundamental formula for the ionization amplitude in the wave treatment (see Ref. [14] for notation):

$$f_{\rm ion} = -\frac{1}{2\pi}\langle e^{i\mathbf{k}_f\cdot\mathbf{R}}\psi_{\boldsymbol{\kappa}}^{-}|V|\Psi^{+}\rangle, \tag{1}$$

where $\psi_{\boldsymbol{\kappa}}^{-}$ is the singly ionized state of the atom [18], $\boldsymbol{\kappa}$ is the momentum of the ejected electron relative to the target nucleus, and $\mathbf{k}_f$ is the final momentum of the projectile relative to the target. By conservation of energy

$$k_f^2 = k_0^2 - \mu(\kappa^2 + 2I), \tag{2}$$

where $\mathbf{k}_0$ is the initial momentum of the projectile relative to the target, μ is the reduced mass of the projectile and target, and I is the ionization potential of the atom.

As in Ref. [14], let ψ_α be the set of atom (eigenstates and) pseudostates. Assuming that the ψ_α approximate a complete set for matrix element purposes, we write

$$\langle e^{i\mathbf{k}_f\cdot\mathbf{R}}\psi_{\boldsymbol{\kappa}}^-|V|\Psi^+\rangle = \sum_\alpha \langle\psi_{\boldsymbol{\kappa}}^-|\psi_\alpha\rangle\langle e^{i\mathbf{k}_f\cdot\mathbf{R}}\psi_\alpha|V|\Psi^+\rangle. \tag{3}$$

The matrix elements

$$\langle e^{i\mathbf{k}_f\cdot\mathbf{R}}\psi_\alpha|V|\Psi^+\rangle \tag{4}$$

are in general off-energy-shell, i.e.,

$$k_f^2 \neq k_0^2 + 2\mu(\varepsilon_0 - \varepsilon_\alpha), \tag{5}$$

where ε_α is the energy of the state ψ_α and where ψ_0 is the initial state of the atom. If the set ψ_α is chosen so that one state from each symmetry (S-, P-, D-, etc.) has exactly the energy

$$\varepsilon_\alpha = \frac{\kappa^2}{2} + I + \varepsilon_0, \tag{6}$$

then for these chosen states (4) will be on-energy-shell. But also, as shown in Ref. [14], for the other states in the set $\langle\psi_{\boldsymbol{\kappa}}^-|\psi_\alpha\rangle$ will be negligibly small. As a result the sum in (3) can then be confined to the specially constructed states, i.e.,

$$\langle e^{i\mathbf{k}_f\cdot\mathbf{R}}\psi_{\boldsymbol{\kappa}}^-|V|\Psi^+\rangle \doteq \sum_{\substack{\alpha \\ \varepsilon_\alpha=\frac{\kappa^2}{2}+I+\varepsilon_0}} \langle\psi_{\boldsymbol{\kappa}}^-|\psi_\alpha\rangle\langle e^{i\mathbf{k}_f\cdot\mathbf{R}}\psi_\alpha|V|\Psi^+\rangle \tag{7}$$

Now every term in the sum (7) is on-energy-shell. This means that we can use the relationship

$$\langle e^{i\mathbf{k}_f\cdot\mathbf{R}}\psi_\alpha|V|\Psi^+\rangle = 2\pi v_0 i^{m_\alpha - m_0 + 1} e^{i(m_0-m_\alpha)\phi_q} \times \int_0^\infty J_{(m_\alpha - m_0)}(q_t b)[\bar{a}_\alpha(\infty, b) - \delta_{\alpha 0}]bdb \tag{8}$$

between the wave and impact parameter treatments which is only valid on-energy-shell. In (8) $\boldsymbol{v}_0 = \mathbf{k}_0/\mu$, m_α is the magnetic quantum number of the state ψ_α relative to $\mathbf{k}_0$ as z axis, $\mathbf{b}$ is the impact parameter, $\bar{a}_\alpha(\infty, b)$ is the impact parameter amplitude for exciting the state ψ_α, and $\mathbf{q}_t$ is the transverse-momentum transfer whose magnitude, dropping terms of order $1/\mu$, is given by

$$q_t^2 = q^2 - \frac{\mu^2(\kappa^2 + 2I)^2}{2\left(k_0^2 + k_f^2\right)}. \tag{9}$$

An inconvenient aspect of the approximation (7) is that a new set of pseudostates has to be constructed for each ejected electron energy and the coupled impact parameter equations re-solved to calculate the $\bar{a}_\alpha$. We here investigate a relaxation of the approximation in which we use (3) and (8) for arbitrary κ and a given fixed set of pseudostates, even though $\langle e^{i\mathbf{k}_f\cdot\mathbf{R}}\psi_\alpha|V|\Psi^+\rangle$ may be off-energy-shell. The approximation is therefore

$$f_{\text{ion}} = -i v_0 \sum_{\text{all}\,\alpha} \langle\psi_{\boldsymbol{\kappa}}^-|\psi_\alpha\rangle i^{m_\alpha - m_0} e^{i(m_0-m_\alpha)\phi_q} \times \int_0^\infty J_{(m_\alpha - m_0)}(q_t b)[\bar{a}_\alpha(\infty, b) - \delta_{\alpha 0}]bdb \tag{10}$$

For H, and He in a frozen core treatment, the pseudostates may be labeled by the hydrogenic quantum numbers nlm [14]. Then (10) becomes

$$f_{\text{ion}} = -\sqrt{\frac{2}{\pi}} i v_0 \sum_l (-i)^l e^{i\eta_l} \times \sum_{m=-l}^{+l} i^{m-m_0} B_{lm}(\kappa, q_t) e^{i(m_0-m)\phi_q} Y_{lm}(\hat{\boldsymbol{\kappa}}), \tag{11}$$

where

$$B_{lm}(\kappa, q_t) \equiv \sum_n b_{nl}(\kappa) C_{nlm}(q_t) \tag{12}$$

$$C_{nlm}(q_t) \equiv \int_0^\infty J_{(m-m_0)}(q_t b)\bar{a}_{nlm}(\infty, b)bdb \tag{13}$$

where η_l is the phase shift for the ejected electron scattering off the ion with angular momentum l, Y_{lm} is a spherical harmonic [19], and $b_{nl}(\kappa)$ gives the distribution of the atom state ψ_{nlm} over the continuum momentum κ of the ejected electron (see Eqs. (53), (57), and (58) of [14]).

B. Cross sections

From (11) the triple differential cross section (TDCS) in the laboratory frame is given by

$$\frac{d^3\sigma^L}{dEd\Omega_e d\Omega_p} = \frac{2}{\pi} v_0 v_f \kappa m_p^2 \sum_l \sum_{l'} i^{l'-l} e^{i(\eta_l - \eta_{l'})} \sum_{m=-l}^{+l} \sum_{m'=-l'}^{+l'} i^{m-m'} \times B_{lm}(\kappa, q_t) B_{l'm'}^*(\kappa, q_t) e^{i(m'-m)\phi_q} Y_{lm}(\hat{\boldsymbol{\kappa}}) Y_{l'm'}^*(\hat{\boldsymbol{\kappa}}), \tag{14}$$

where m_p is the mass of the projectile and $*$ denotes complex conjugation.

Integration of (14) over $d\Omega_e (\equiv d\hat{\boldsymbol{\kappa}})$ gives the double differential cross section (DDCS)

$$\frac{d^2\sigma^L}{dEd\Omega_p} = \frac{2}{\pi} v_0 v_f \kappa m_p^2 \sum_l \sum_{m=-l}^{+l} |B_{lm}(\kappa, q_t)|^2, \tag{15}$$

again as observed in the laboratory frame. Usually more useful than (15) is the DDCS $d^2\sigma/dEdq$ which is easily obtained from (15) as

$$\frac{d^2\sigma}{dEdq} = 4\kappa q \sum_l \sum_{m=l}^{+l} |B_{lm}(\kappa, q_t)|^2. \tag{16}$$

Integrating (14) over $d\Omega_p$ gives [20]

$$\frac{d^2\sigma}{dEd\Omega_e} = 4\kappa \int_0^\infty q_t dq_t \sum_l \sum_{l'} i^{l'-l} e^{i(\eta_l - \eta_{l'})} \times \sum_{m=-\mathrm{Min}(l,l')}^{+\mathrm{Min}(l,l')} B_{lm}(\kappa, q_t) B^*_{l'm}(\kappa, q_t) P_{lm}(\theta_e) P_{l'm}(\theta_e), \tag{17}$$

where θ_e is the polar ejection angle of the electron and P_{lm} is an associated Legendre function [19], and where we have taken the upper limit on q_t to be ∞ since the largest possible value of q_t is of $O(\mu)$.

Integrating (15) with respect to E we obtain

$$\frac{d\sigma^L}{d\Omega_p} = \frac{2}{\pi} v_0 m_p^2 \int_0^{\kappa_{\max}} v_f(\kappa) \left[\sum_{lm} |B_{lm}(\kappa, q_t(\kappa))|^2 \right] \kappa^2 d\kappa \tag{18}$$

where, from (2),

$$\kappa^2_{\max} = \frac{k_0^2}{\mu} - 2I. \tag{19}$$

As indicated by the notations $v_f(\kappa)$ and $q_t(\kappa)$ in (18), v_f and q_t are to be taken as functions of κ given by

$$v_f(\kappa) = \sqrt{v_0^2 - \frac{(\kappa^2 + 2I)}{\mu}} \tag{20}$$

and (9). In (9) q must be evaluated for fixed θ_p^L, where θ_p^L is the laboratory scattering angle of the projectile. Now

$$q^2 = k_0^2 + k_f^2 - 2k_0 k_f \cos\theta_p \tag{21}$$

but where θ_p is the scattering angle of the projectile in the relative coordinate system. With a little algebra it can be shown that [20]

$$\cos\theta_p = -\left(\frac{m_p}{\mu} - 1\right) \frac{v_0}{v_f} \left(1 - \left(\cos\theta_p^L\right)^2\right) + \cos\theta_p^L \left[1 + \left(\left(\cos\theta_p^L\right)^2 - 1\right) \left(\frac{m_p}{\mu} - 1\right)^2 \frac{v_0^2}{v_f^2}\right]^{\frac{1}{2}}. \tag{22}$$

The results (2), (9), (20), (21), and (22) then define q_t as a function of κ for fixed θ_p^L, as required in (18).

By integrating (16) over $dE = \kappa d\kappa$ we can calculate $d\sigma/dq$. We get

$$\frac{d\sigma}{dq} = 4q \sum_l \sum_{m=-l}^{+l} \int_0^{\kappa_{\max}(q)} |B_{lm}(\kappa, q_t(\kappa))|^2 \kappa^2 d\kappa, \tag{23}$$

where q_t is to be treated as a function of κ for fixed q defined by (9). The upper limit $\kappa_{\max}(q)$ is obtained from (9) by setting $q_t = 0$ and dropping terms of order $1/\mu$. We get

$$\kappa_{\max}(q) = \sqrt{2v_0 q - 2I}. \tag{24}$$

By integrating (16) over q (equivalently q_t) at fixed κ we get

$$\frac{d\sigma}{dE} = 4\kappa \sum_l \sum_{m=-l}^{+l} \int_0^\infty |B_{lm}(\kappa, q_t)|^2 q_t dq_t. \tag{25}$$

By integrating (17) over E we obtain

$$\frac{d\sigma}{d\Omega_e} = 4 \sum_l \sum_{l'} \sum_{m=-\mathrm{Min}(l,l')}^{+\mathrm{Min}(l,l')} i^{l'-l} \times \left\{ \int_0^{\kappa_{\max}} e^{i(\eta_l(\kappa) - \eta_{l'}(\kappa))} D_{ll'm}(\kappa) \kappa^2 d\kappa \right\} P_{lm}(\theta_e) P_{l'm}(\theta_e), \tag{26}$$

where $\kappa_{\max}$ is given in (19), quantities that depend on κ are indicated by the addition of "(κ)," and where we define

$$D_{ll'm}(\kappa) \equiv \int_0^\infty B_{lm}(\kappa, q_t) B^*_{l'm}(\kappa, q_t) q_t dq_t. \tag{27}$$

In Ref. [14] we used the prescription

$$\sigma_{\mathrm{ion}} = \sum_{\text{all nlm}} g_{nl} \sigma_{nlm} \tag{28}$$

to calculate the total (single) ionization cross section. Here σ_{nlm} is the cross section for exciting the state ψ_{nlm} and

$$g_{nl} = \frac{2}{\pi} \int_0^\infty |b_{nl}(\kappa)|^2 \kappa^2 d\kappa \tag{29}$$

is the fraction of this state overlapping the continuum. The approximation (28) is a more refined version of that normally used, e.g., Refs. [21–24], where g_{nl} is taken to be unity for states ψ_{nlm} with energy ε_{nl} above the ionization threshold and zero otherwise. No direct connection between the differential theory and the prescription (28) was established. We now show how (28) follows from the relaxed approximation (11) and what further approximations are needed to make the connection. We can start from any of (18), (23), (25) or (26) [20]. We choose (25). Integrating (25) over E we get

$$\sigma_{\mathrm{ion}} = 4 \sum_l \sum_{m=-l}^{+l} \int_0^\infty \kappa^2 d\kappa \left[\int_0^\infty |B_{lm}(\kappa, q_t)|^2 q_t dq_t \right]. \tag{30}$$

Technically, the upper limit of the κ integration is given by (19) but since this is of $O(\mu^{1/2})$ we can, to all intents and purposes, take it as ∞. Now consider

$$\int_0^\infty |B_{lm}(\kappa, q_t)|^2 q_t dq_t = \sum_n \sum_{n'} b_{nl}(\kappa) b^*_{n'l}(\kappa) \int_0^\infty C_{nlm}(q_t) C^*_{n'lm}(q_t) q_t dq_t. \tag{31}$$

From (13)

$$\int_0^\infty C_{nlm}(q_t) C^*_{n'lm}(q_t) q_t dq_t = \int_0^\infty q_t dq_t \int_0^\infty b db \int_0^\infty b' db' \times J_{(m-m_0)}(q_t b) \times J_{(m-m_0)}(q_t b') \bar{a}_{nlm}(\infty, b) \bar{a}^*_{n'lm}(\infty, b'). \tag{32}$$

Using the Hankel transform result [25]

$$\int_0^\infty J_\nu(q_t b)J_\nu(q_t b')q_t dq_t = \frac{1}{b}\delta(b-b') \tag{33}$$

(32) becomes

$$\int_0^\infty \bar{a}_{nlm}(\infty,b)\bar{a}^*_{n'lm}(\infty,b)bdb. \tag{34}$$

Using (31) and (34) in (30) we therefore get

$$\sigma_{\rm ion} = 4\sum_l \sum_{m=-l}^{+l} \sum_n \sum_{n'} \left[\int_0^\infty \bar{a}_{nlm}(\infty,b)a^*_{n'lm}(\infty,b)bdb\right] \times \left[\int_0^\infty b_{nl}(\kappa)b^*_{n'l}(\kappa)\kappa^2 d\kappa\right]. \tag{35}$$

So far no approximations have been made. Now, from Eq. (53) of [14]

$$\int_0^\infty b_{nl}(\kappa)b^*_{n'l}(\kappa)\kappa^2 d\kappa = \frac{\pi}{2}\int \langle\psi_{nlm}|\psi^-_{\boldsymbol{\kappa}}\rangle\langle\psi^-_{\boldsymbol{\kappa}}|\psi_{n'lm}\rangle d\boldsymbol{\kappa}. \tag{36}$$

If the continuum eigenstates $\psi^-_{\boldsymbol{\kappa}}$ formed a complete set, which they do not since we need the bound eigenstates for a complete set, (36) would give

$$\int_0^\infty b_{nl}(\kappa)b^*_{n'l}(\kappa)\kappa^2 d\kappa = \frac{\pi}{2}\delta_{nn'}. \tag{37}$$

Let us now make the approximation that (37) holds for $n \neq n'$. Then using (29), (35) becomes

$$\sigma_{\rm ion} = 4\sum_{nlm}\left[\int_0^\infty |b_{nl}(\kappa)|^2\kappa^2 d\kappa\right]\left[\int_0^\infty |\bar{a}_{nlm}(\infty,b)|^2 bdb\right] = \sum_{nlm} g_{nl}\sigma_{nlm}. \tag{38}$$

The result (28) is therefore established with a little further approximation beyond that used for the differential cross sections. Where the pseudostates ψ_{nlm} and $\psi_{n'lm}$ lie almost completely in the continuum ($g_{nl} \approx 1$), which is mostly the case, this further approximation will be negligible.

The derivation of the result (38) from (18) leads to an interesting and "sensible" formula [20]. First note from (22) that fixed θ_p^L implies fixed θ_p to within corrections of $O(1/\mu)$. From (9) it can be shown that

$$q_t^2 = 2k_0^2\left(1+O\left(\frac{1}{\mu}\right)\right)(1-\cos\theta_p) + O\left(\frac{1}{\mu}\right). \tag{39}$$

Now $B_{lm}(\kappa, q_t)$ becomes negligible whenever either κ or q_t become "large." From (20) and (39) this implies that we may as well take $v_f(\kappa) = v_f(0)$ and $q_t(\kappa) = q_t(0)$ and $\kappa_{\max} = \infty$ so that (18) becomes

$$\frac{d\sigma^L}{d\Omega_p} = \frac{2}{\pi}v_0 v_f(0)m_p^2\int_0^\infty\left(\sum_{l,m}|B_{lm}(\kappa, q_t(0))|^2\right)\kappa^2 d\kappa. \tag{40}$$

Then, making the approximation (37) for $n \neq n'$ we get

$$\frac{d\sigma^L}{d\Omega_p} = v_0 v_f(0)m_p^2\sum_{nlm} g_{nl}|C_{nlm}(q_t(0))|^2. \tag{41}$$

Using the same arguments that led from (18) to (40), we might equally well take $v_f(0)$ to be v_{nl} and $q_t(0)$ to be $(q_t)_{nl}$, where

$$v_{nl} = \frac{k_{nl}}{\mu} \tag{42a}$$

$$k_{nl}^2 = k_0^2 + 2\mu(\varepsilon_0 - \varepsilon_{nl}) \tag{42b}$$

$$q_{nl}^2 = k_0^2 + k_{nl}^2 - 2k_0 k_{nl}\cos\theta_p \tag{42c}$$

$$(q_t)_{nl}^2 = q_{nl}^2 - \frac{2\mu^2(\varepsilon_0-\varepsilon_{nl})^2}{k_0^2+k_{nl}^2}, \tag{42d}$$

these being the values of v_f, q^2, and q_t^2 appropriate to excitation of the discrete (pseudo)state ψ_{nlm}. Then recognizing that the laboratory differential cross section for exciting the state ψ_{nlm} is (see Ref. [14])

$$\frac{d\sigma^L_{nlm}}{d\Omega_p} = v_0 v_{nl} m_p^2 |C_{nlm}((q_t)_{nl})|^2, \tag{43}$$

we obtain the "sensible" result

$$\frac{d\sigma^L}{d\Omega_p} = \sum_{nlm} g_{nl}\frac{d\sigma^L_{nlm}}{d\Omega_p} \tag{44}$$

from which (28) follows trivially by integration over Ω_p.

III. TESTING THE RELAXED APPROXIMATION

We begin with a first Born test. This has been made by using the first Born approximation $\bar{a}^{B1}_{nlm}(\infty,b)$ to $\bar{a}_{nlm}(\infty,b)$ to calculate the functions $C_{nlm}(q_t)$ of (13). Following [14] we label this approximation IPMB1. We have then compared the results of IPMB1 with exact first Born calculations (EXB1). For simplicity, we have confined the test to an atomic hydrogen target where there is an exact analytic expression for the first Born TDCS (see Ref. [14]). We have used the 165 state basis set of [14] for the pseudostates in IPMB1. As described in Ref. [14], this set has been constructed so that the $n = 10$ states have an energy of 5 eV exactly. As a result, the relaxed approximation (10) will coincide with the more rigorous approximation (7) whenever the ejected energy is 5 eV. In order to keep the comparison within reasonable bounds we tested only the single and double differential cross sections and then, of necessity, only for a selection of impact energies (2, 10, and 30 keV) and ejected electron energies (1, 5, 10, 20, 30, and 50 eV). We take the view that calculations of the more detailed TDCS will usually be made using the more robust approximation (7).

The full results of our first Born test are reported in [20]. Suffice it to say that, generally, we got very good agreement between IPMB1 and EXB1. In Figs. 1 and 2 we show two typical examples. Only in the colored online versions of these figures is it obvious that there are two sets of curves, IPMB1 and EXB1, present.

We have also tested the relaxed approximation under extreme nonperturbative conditions, namely for Au^{24+} and Au^{53+} impact on He at 3.6 MeV/amu. The full set of tests may be viewed in Ref. [20]. Again, within the context of the test, we found very good performance of the relaxed approximation. The worst case we encountered is shown in Fig. 3. The nature of the test was to take two sets of pseudostates, each of 165

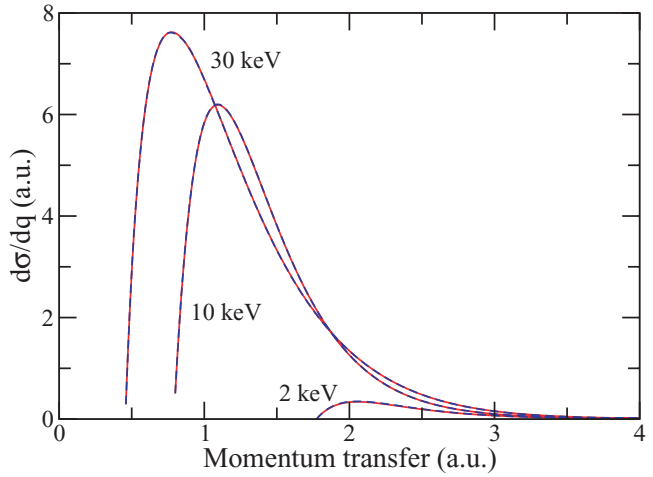

FIG. 1. (Color online) First Born single differential cross section $d\sigma/dq$ for antiproton impact ionization of H at impact energies of 2, 10, and 30 keV: red solid curve, EXB1; blue dashed curve, IPMB1.

states. One set was adapted to electron ejection at 4 eV, the other to ejection at 10 eV (these were similar to the 5-eV set of He states used in Ref. [14]). We performed full coupled pseudostate calculations with both and made comparisions of $d^2\sigma/dEdq$ and $d^2\sigma/dEd\Omega_e$ for ejected energies of 4 and 10 eV and of $d\sigma/dq$, $d\sigma/dE$, and $d\sigma/d\Omega_e$. It is the latter which is shown in Fig. 3 for Au^{53+} impact. While we now see a difference between the two results, that difference is comparatively small.

In conclusion, on the basis of the tests so far made, we believe that the relaxed approximation is very viable. However, it must be recognized that these tests are, of necessity, somewhat limited and so caution needs to be exercised until wider experience with the relaxed approximation is obtained.

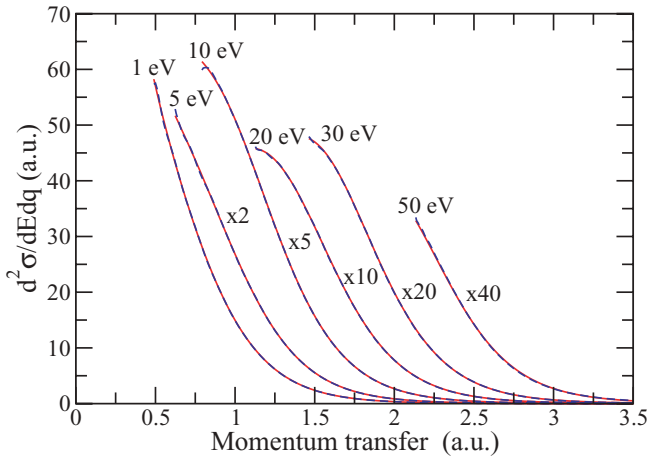

FIG. 2. (Color online) First Born cross section $d^2\sigma/dEdq$ for antiproton impact ionization of H at an impact energy of 30 keV and for ejected electron energies ranging from 1 to 50 eV: red solid curve, EXB1; blue dashed curve, IPMB1. The curves for 5 eV and above have been scaled up by the indicated factors.

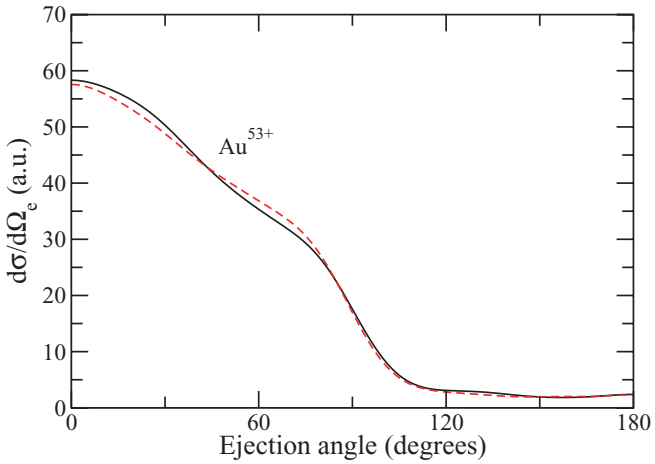

FIG. 3. (Color online) $d\sigma/d\Omega_e$ for Au^{53+} impact ionization of He at 3.6 MeV/amu as calculated in the full impact parameter coupled pseudostate approximation [26]: black solid curve, using the 165 pseudostate set adapted to 4 eV ejection; red dashed curve, using the 165 pseudostate set adapted to 10 eV ejection.

IV. RESULTS

We report results for antiproton impact ionization of H and He using the relaxed approximation (11). For our full impact parameter coupled pseudostate calculations (CP) we have used the 165 state sets described in Ref. [14]. As a benchmark, we also make some comparisions with corresponding first Born numbers. In the case of H, the first Born results are exact (EXB1), in the case of He they have been obtained from the first Born version of (11) (IPMB1) using the 165 pseudostate set. We have chosen the more interesting lower impact energies to illustrate our calculations: 2, 10, and 30 keV for H; 3, 12, and 60 keV for He.

A. Atomic hydrogen target

In Fig. 4 we show the double differential cross section (DDCS) $d^2\sigma/dEdq$ at an impact energy of 2 keV and for

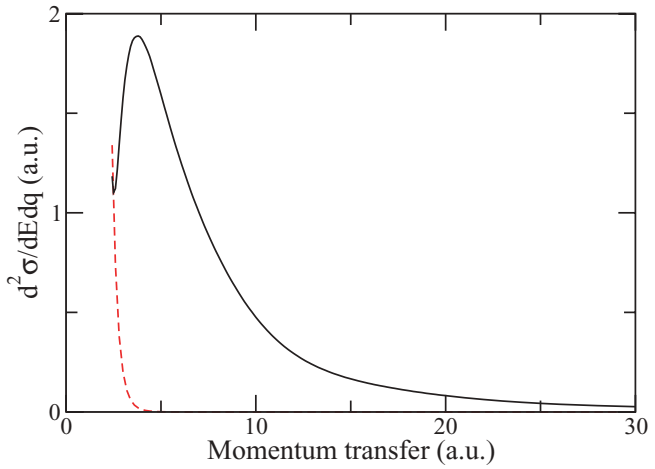

FIG. 4. (Color online) Cross section $d^2\sigma/dEdq$ for antiproton ionization of H at an impact energy of 2 keV and for an ejected electron energy of 5 eV: solid curve, CP approximation; dashed curve, EXB1 approximation.

an ejected electron energy of 5 eV [27]. We see that with increasing momentum transfer q the CP cross section initially falls rapidly but then quickly reaches a sharp minimum followed by a large maximum and a sustained cross section out to momentum transfers as large as 30 a.u.. By contrast, the corresponding first Born cross section just declines rapidly with increasing q. The difference between the two results is attributed to the interaction between the projectile and the target nucleus in the CP approximation and its absence from the first Born approximation (FBA). In its initial fall the CP approximation is like the FBA and so in this stage it is presumed that long range effects, which are taken into account in the FBA, are dominant. However, the quick divergence of the two approximation with increasing q attests to the rapid onset of nuclear dominance. In Fig. 5(a) we show the same CP cross section at 2 keV but now for a range of ejected energies up to 8 eV. In this picture we see a more dramatic representation of the changeover from long range to nuclear scattering, namely a pronounced crease in the cross-section surface. However, as Fig. 5(b) shows, by 10 keV the crease has disappeared and it is no longer possible to see a visual separation between long range and nuclear scattering, they have merged into a continuum. Figure 5(c), for an impact energy of 30 keV, is similar to Fig. 5(b) but shows a more rapid rate of fall of cross section with both ejected energy and q.

Figure 6 shows the CP results for $d^2\sigma/dEd\Omega_e$. At all three impact energies we see strong backward repulsion of low-energy ejected electrons, the more so with reducing impact energy.

Figure 7 shows $d\sigma/dq$ at the selected impact energies both in the CP approximation and in the first Born EXB1 approximation. The area under these curves gives the total ionization cross section shown in Fig. 2 of Ref. [14]. At 2 keV, Fig. 7(a), the EXB1 cross section is dwarfed by the CP aproximation as we would expect from the total ionization cross section where EXB1 is very small in comparision with CP. As discussed above, the difference beween the two is due to nuclear scattering. The effect of nuclear scattering is also seen in Figs. 7(b) and 7(c) for impact energies of 10 and 30 keV, respectively. The result of the nuclear interaction is to give a CP cross section which exceeds EXB1 with increasing momentum transfer even though the total ionization cross section in EXB1 may be signifcantly larger than the corresponding CP cross section, which is the case at 30 keV (see Fig. 2 of Ref. [14]). Where the EXB1 total ionization cross section is comparable to or larger than CP, as is the case at 10 or 30 keV, this means that the EXB1 differential cross section must substantially exceed its CP counterpart at the lower momentum transfers since it has to be squeezed into a smaller momentum range; see Figs. 7(b) and 7(c). It should be noted that, unlike the cross section $d^2\sigma/dEdq$ which is finite at minimum momentum transfer (see Figs. 4 and 5), the cross section $d\sigma/dq$ is zero at its minimum momentum transfer of $q = I/v_0$ (see (23) and (24)).

Figure 8 shows $d\sigma/d\Omega_e$. At 2 keV the CP approximation shows $d\sigma/d\Omega_e$ to be strongly peaked for backward ejection, as we would expect from Fig. 6(a). However, by 10 keV the CP cross section, while still largest at the backward direction, is more flat. By 30 keV the CP $d\sigma/d\Omega_e$ displays a shallow maximum just above 60°, a shallow minimum just below

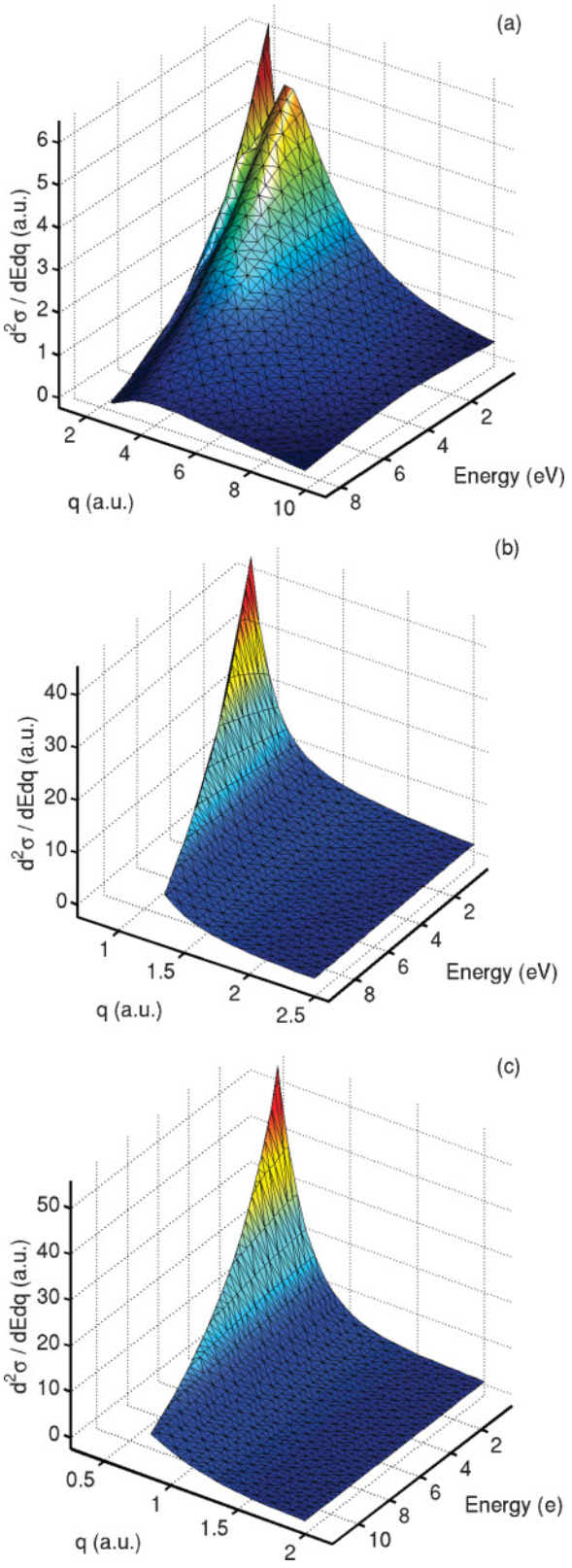

FIG. 5. (Color online) $d^2\sigma/dEdq$ for antiproton ionization of H at impact energies of (a) 2 keV, (b) 10 keV, and (c) 30 keV, as calculatd in the CP approximation.

120°, and a small rise toward the backward direction. At first sight, this might not be immediately expected from Figs. 6(b) and 6(c) with their large backward peaked cross sections at

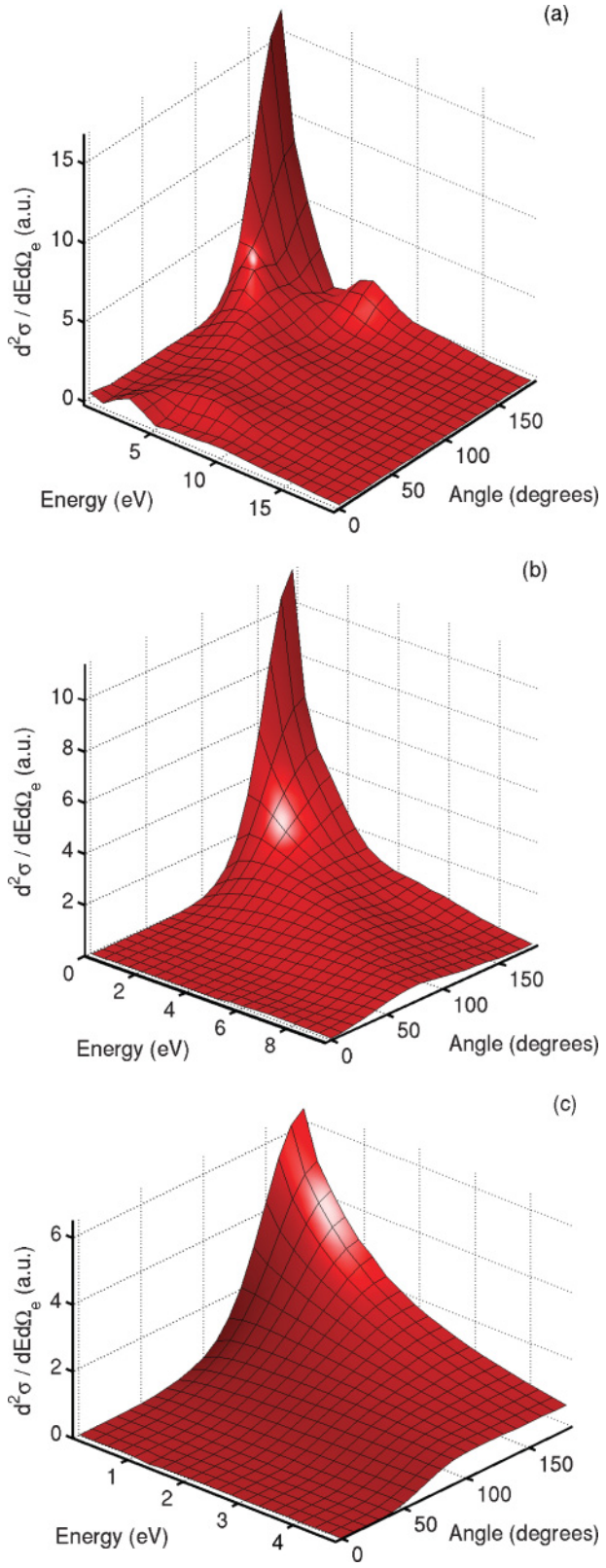

FIG. 6. (Color online) $d^2\sigma/dEd\Omega_e$ for antiproton ionization of H at impact enegies of (a) 2 keV, (b) 10 keV, and (c) 30 keV, as calculated in the CP approximation.

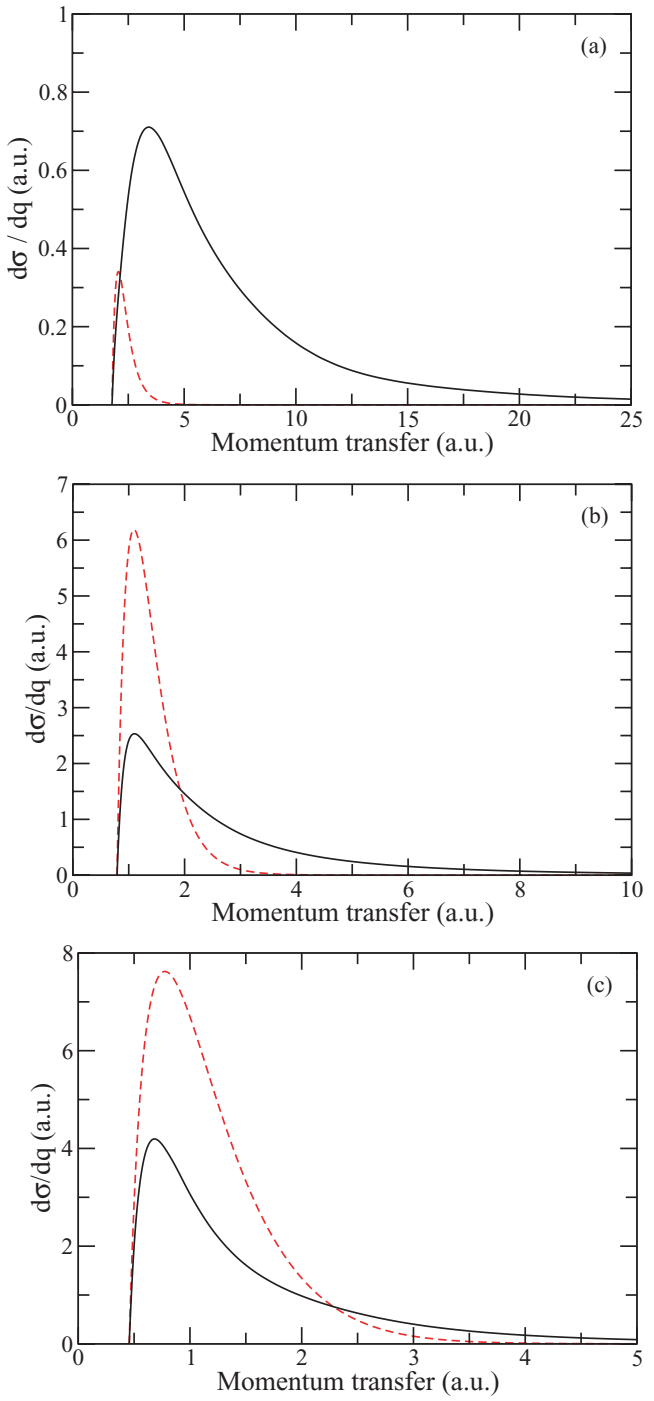

FIG. 7. (Color online) $d\sigma/dq$ for antiproton ionization of H at impact energies of (a) 2 keV, (b) 10 keV, and (c) 30 keV: solid curve, CP approximation; dashed curve, EXB1 approximation.

low ejection energies. However, we shall see below that with increasing impact energy the higher ejected electron energies are proportionately a larger contribution to the cross section. In the integral over all ejected electron energies that transforms $d^2\sigma/dEd\Omega_e$ into $d\sigma/d\Omega_e$, therefore, the contribution from the higher energies tones down that from the low ejected energy region. The first Born approximation, not shown (see Ref. [20]), is unrealistic at the impact energies of Fig. 8. It has a forward peak and decreases monotonically with increasing angle.

Finally, Fig. 9 shows $d\sigma/dE$. At 10 and 30 keV the CP cross section, like the first Born cross section (not shown,

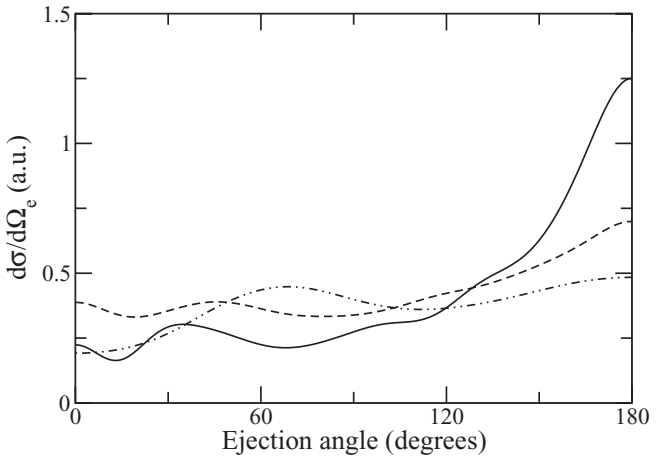

FIG. 8. (Color online) $d\sigma/d\Omega_e$ in the CP approximation for antiproton ionization of H at impact energies of 2 keV (solid curve), 10 keV (dashed curve), and 30 keV (dash double-dot curve).

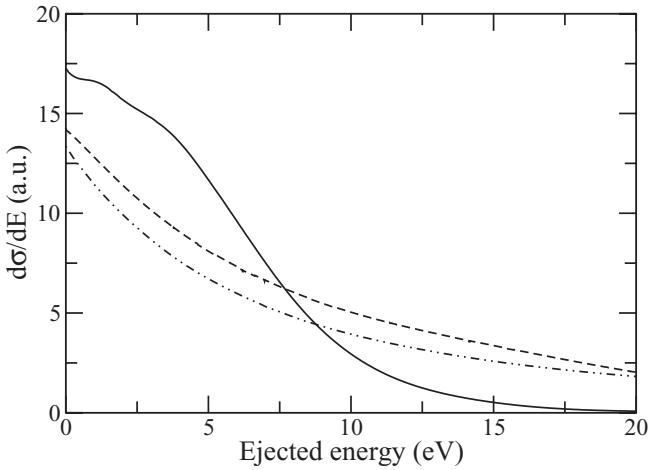

FIG. 9. (Color online) $d\sigma/dE$ in the CP approximation for antiproton ionization of H at impact energies of 2 keV (solid curve), 10 keV (dashed curve), and 30 keV (dash double-dot curve).

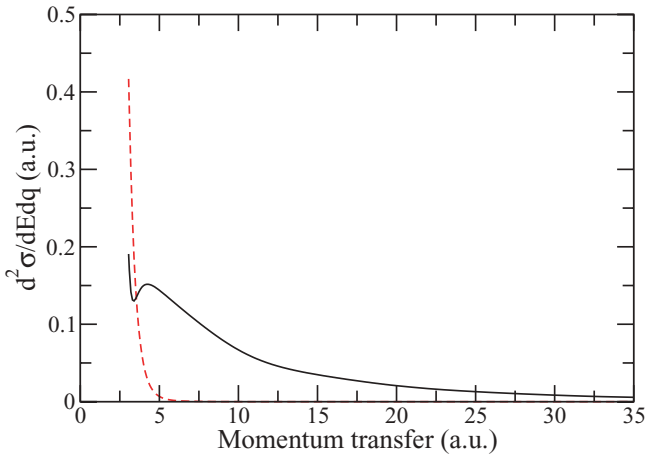

FIG. 10. (Color online) Cross section $d^2\sigma/dEdq$ for antiproton ionization of He at an impact energy of 3 keV and for an ejected energy of 5 eV: solid curve, CP approximation; dashed curve, first Born IPMB1 approximation.

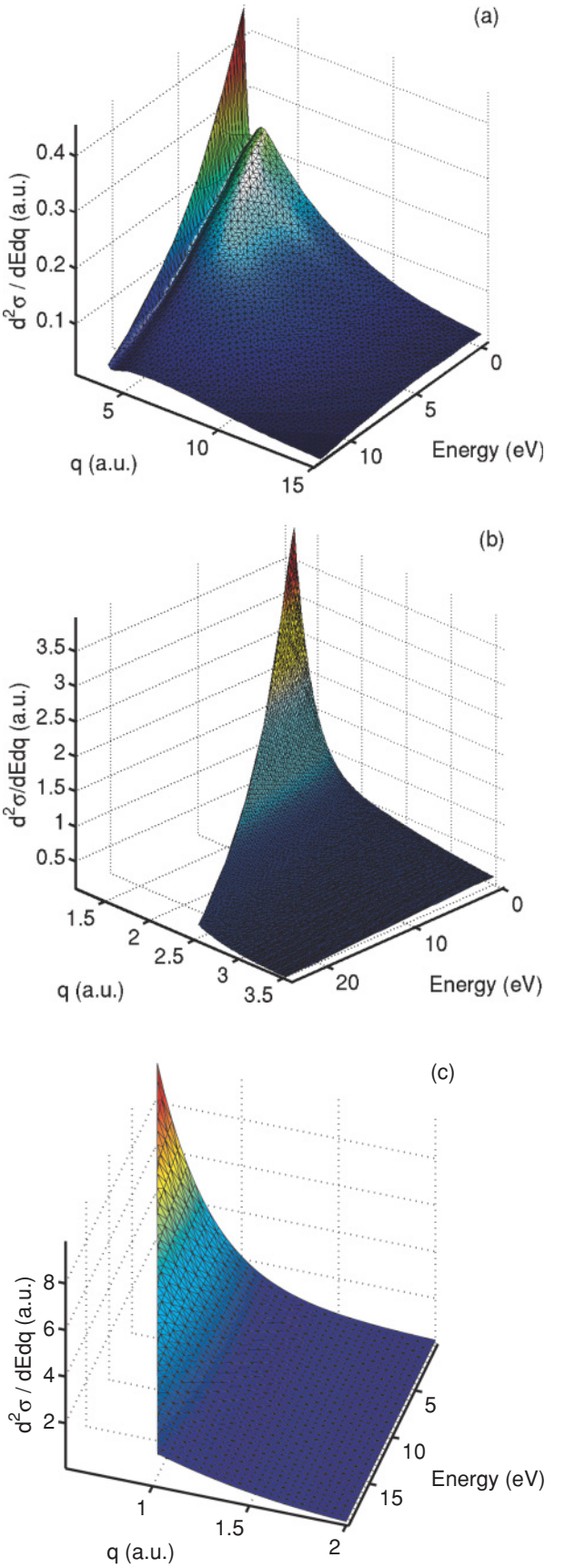

FIG. 11. (Color online) $d^2\sigma/dEdq$ for antiproton ionization of He at impact energies of (a) 3 keV, (b) 12 keV, and (c) 60 keV, as calculated in the CP approximation.

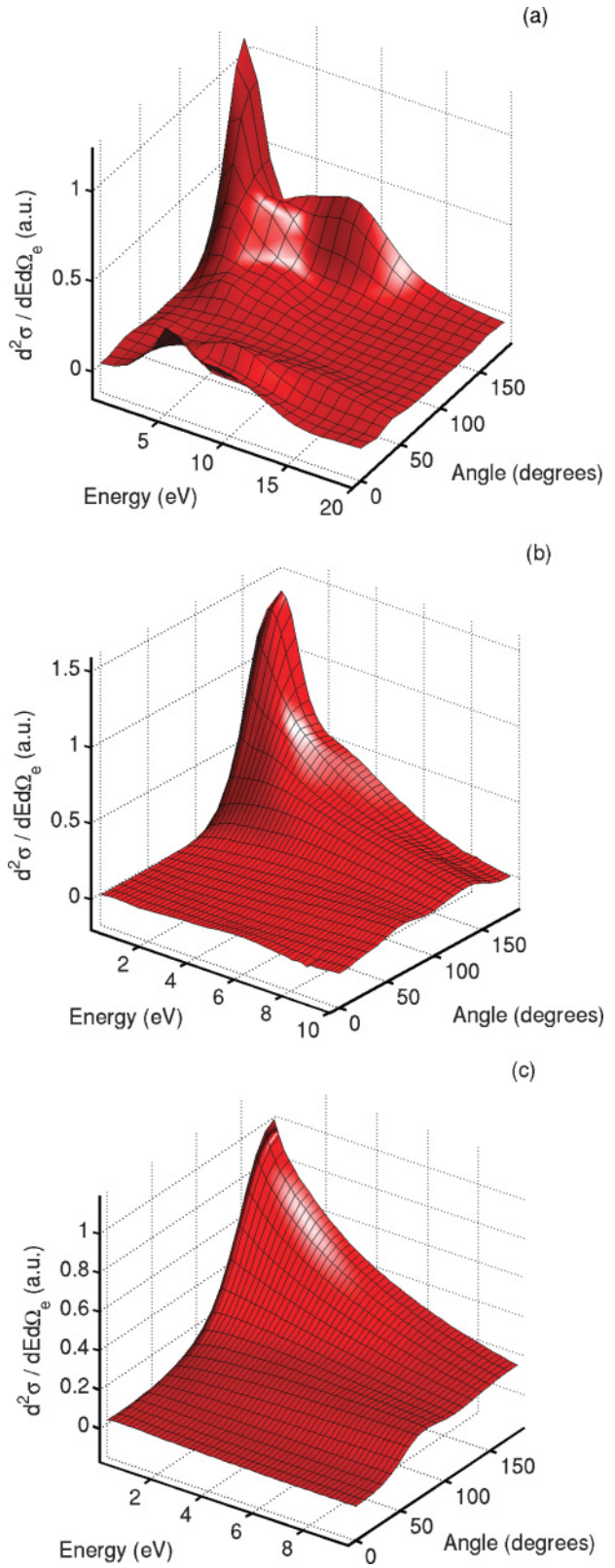

FIG. 12. (Color online) $d^2\sigma/dEd\Omega_e$ for antiproton ionization of He at impact energies of (a) 3 keV, (b) 12 keV, and (c) 60 keV, as calculated in the CP approximation.

see Ref. [20]) is concave downward. This is a feature of the higher impact energy regime. By contrast, at 2 keV, the CP cross section is mainly convex upward at the lower energies. It

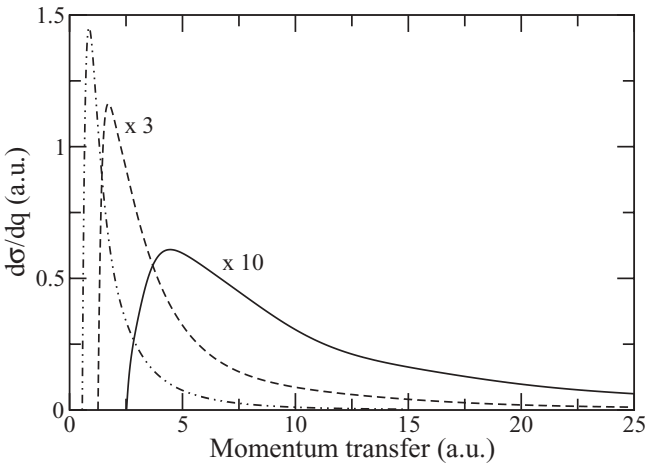

FIG. 13. $d\sigma/dq$ in the CP approximation for antiproton ionization of He at impact energies of 3 keV (solid curve), 12 keV (dashed curve), and 60 keV (dash double-dot curve).

should be noted that, with increasing impact energy, the higher ejected energies are proportionately a larger contribution to $d\sigma/dE$.

B. Helium target

In Figs. 10 to 15 we show results for a He target at impact energies of 3, 12, and 60 keV. Since He is experimentally a more feasible target than H, it is the target whose differential scattering is most likely to be first studied. We see the same kind of patterns as in Figs. 4 to 9 for H. In Figs. 10 and 11(a) for $d^2\sigma/dEdq$ we observe the same "crease" in the low-energy 3-keV cross section as was seen in the 2-keV cross section for H [Figs. 4 and 5(a)], once more associated with the transition from dominant long-range interaction to dominant short-range nuclear scattering. Figure 12 for $d^2\sigma/dEd\Omega_e$ mirrors Fig. 6 for H, except that there is more structure in the He cross section. Whether this increased structure is real or an artifact of the frozen core approximation in unclear at this moment. The greater structure in the He results is again reflected in the comparison between Figs. 14 and 8 for $d\sigma/d\Omega_e$.

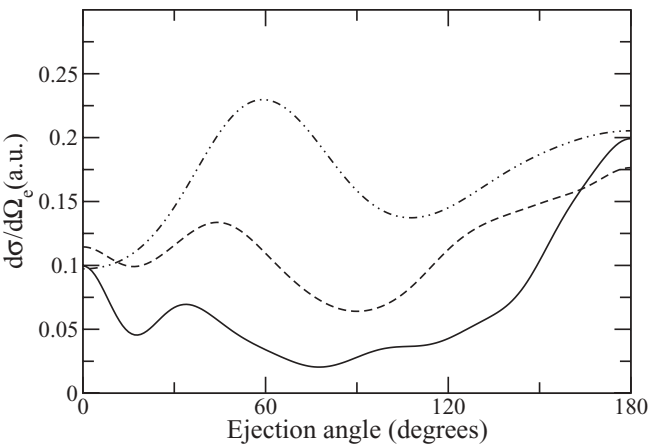

FIG. 14. $d\sigma/d\Omega_e$ in the CP approximation for antiproton ionization of He at impact energies of 3 keV (solid curve), 12 keV (dashed curve), and 60 keV (dash double-dot curve).

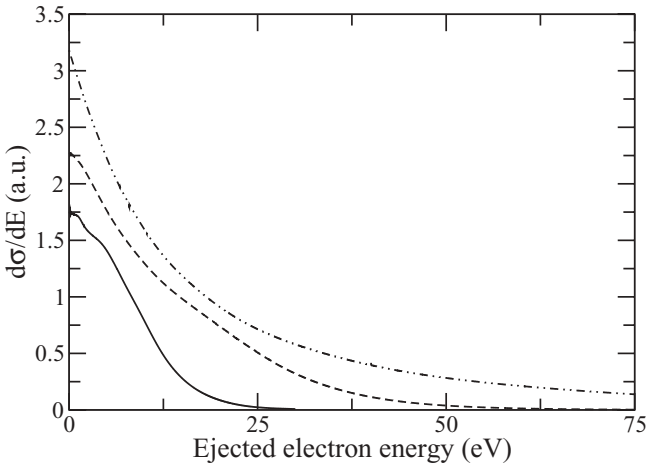

FIG. 15. $d\sigma/dE$ in the CP approximation for antiproton ionization of He at impact energies of 3 keV (solid curve), 12 keV (dashed curve), and 60 keV (dash double-dot curve).

V. CONCLUSIONS

In this article we have investigated a relaxed form (10) of the approximation introduced in Ref. [14]. The relaxation involves the assumption that off-energy-shell amplitudes for exciting pseudostates may be replaced by their on-energy-shell counterparts with little loss of accuracy. Whereas the original approximation of Ref. [14] required the generation of a new set of pseudostates for each ejected electron energy, and the solution of corresponding coupled equations each time, the relaxed approximation needs only a single set of pseudostates, and a single solution of the coupled equations, a considerable saving in computation in situations where a range of ejected energies is required. In a number of tests, both at the first Born and coupled pseudostate levels, we have found that the relaxed approximation appears to lead to little loss of accuracy.

We have also shown how the relaxed approximation leads, with a little further approximation, to the prescription (28) for the total ionization cross section. This prescription, usually in a cruder form where $g_{nl} = 1$ for pseudostates above the ionization threshold and $g_{nl} = 0$ otherwise, is often used in the calculation of total ionization cross sections.

Finally, we have applied the relaxed approximation to antiproton ionization of H and He to generate results of present [13] and future [12] experimental interest. The calculations nicely illustrate two important effects, the role of the interaction between the antiproton and the target nucleus at low energies, Figs. 5 and 11, and the effect of postcollisional interaction between the antiproton and the outgoing ejected electron, Figs. 6 and 12.

ACKNOWLEDGMENTS

One of us (M.M.) acknowledges support from the European Social Fund and Queen's University Belfast. D.A. and J.R.M. acknowledge financial support from the Brazilian agencies CNPq, Capes, and Fapemig.

[1] H. Knudsen, J. Phys.: Conf. Ser. **194**, 012040 (2009).
[2] H. Knudsen, H.-P. E. Kristiansen, H. D. Thomsen, U. I. Uggerhøj, T. Ichioka, S. P. Møller, C. A. Hunniford, R. W. McCullough, M. Charlton, N. Kuroda, Y. Nagata, H. A. Torii, Y. Yamazaki, H. Imao, H. H. Andersen, and K. Tőkesi, Phys. Rev. Lett. **101**, 043201 (2008).
[3] H. Knudsen, H-P. E. Kristiansen, H. D. Thomsen, U. I. Uggerhøj, T. Ichioka, S. P. Møller, C. A. Hunniford, R. W. McCullough, M. Charlton, N. Kuroda, Y. Nagata, H. A. Torii, Y. Yamazaki, H. Imao, H. H. Andersen, and K. Tőkesi, Nucl. Instrum. Methods B **267**, 244 (2009).
[4] http://www.gsi.de/fair/.
[5] Facility for Low-Energy Antiproton and Ion Research: http://www.oeaw.ac.at/smi/flair/.
[6] Stored Particle Atomic Research Collaboration: http://www.gsi.de/fair/experiments/sparc/.
[7] M. Charlton, J. Eades, D. Horváth, R. J. Hughes, and C. Zimmermann, Phys. Rep. **241**, 65 (1994).
[8] L. V. Jørgensen *et al.* (ALPHA Collaboration), Nucl. Instrum. Methods B **266**, 357 (2008).
[9] G. Gabrielse *et al.* (ATRAP Collaboration), Phys. Rev. Lett. **100**, 113001 (2008).
[10] A. Kellerbauer *et al.* (AEGIS Collaboration), Nucl. Instrum. Methods B **266**, 351 (2008).
[11] H. V. Knudsen *et al.* (CERN ACE Collaboration), Nucl. Instrum. Methods B **266**, 530 (2008).
[12] C. P. Welch, M. Grieser, A. Dorn, R. Moshammer, and J. Ullrich, AIP Conf. Proc. **796**, 266 (2005).
[13] Y. Yamazaki (private communication).
[14] M. McGovern, D. Assafrão, J. R. Mohallem, Colm T. Whelan, and H. R. J. Walters, Phys. Rev. A **79**, 042707 (2009).
[15] Kh. Khayyat, T. Weber, R. Dörner, M. Achler, V. Mergel, L. Spielberger, O. Jagutzki, U. Meyer, J. Ullrich, R. Moshammer, W. Schmitt, H. Knudsen, U. Mikkelsen, R. Aggerholm, E. Uggerhoej, S. P. Moeller, V. D. Rodríguez, S. F. C. O'Rourke, R. E. Olsen, P. D. Fainstein, J. H. McGuire, and H. Schmidt-Böcking, J. Phys. B **32**, L73 (1999).
[16] D. Fischer, A. B. Voitkiv, R. Moshammer, and J. Ullrich, Phys. Rev. A **68**, 032709 (2003).
[17] M. Schulz, M. Dürr, B. Najjari, R. Moshammer, and J. Ullrich, Phys. Rev. A **76**, 032712 (2007).
[18] We suppress the index "i" used in Ref. [14] to label the final state of the ion.
[19] M. E. Rose, *Elementary Theory of Angular Momentum* (Wiley, New York, 1957).
[20] M. McGovern, Ph.D. thesis, Queen's University Belfast, 2009.

[21] B. Pons, Phys. Rev. Lett. **84**, 4569 (2000).
[22] A. Igarashi, S. Nakazaki, and A. Ohsaki, Phys. Rev. A **61**, 062712 (2000).
[23] J. Azuma, N. Toshima, K. Hino, and A. Igarashi, Phys. Rev. A **64**, 062704 (2001).
[24] S. Sahoo, S. C. Mukherjee, and H. R. J. Walters, J. Phys. B **37**, 3227 (2004).
[25] *Bateman Manuscript Project, Volume 2*, edited by A. Erdélyi, W. Magnus, F. Oberhettinger, and F. G. Tricomi (McGraw-Hill, New York, 1954).
[26] M. McGovern, D. Assafrão, J. R. Mohallem, Colm T. Whelan, and H. R. J. Walters, Phys. Rev. A (to be published).
[27] This is an improved calculation of the cross section shown in Fig. 5 of Ref. [14].